Dynamics of Intramolecular Hydrogen-Atom Migrations in 2-Hydroxy-3-nitropyridine Studied by Low-Temperature Matrix-Isolation Infrared Spectroscopy and Density Functional Theory Calculation

Maki Nagaya and Munetaka Nakata*

Graduate School of BASE (Bio-Applications and Systems Engineering), Tokyo University of Agriculture and Technology, Naka-cho, Koganei, Tokyo 184-8588, Japan

Received: April 5, 2007; In Final Form: May 17, 2007

Intramolecular hydrogen-atom migrations in 2-hydroxy-3-nitropyridine have been investigated by low-temperature matrix-isolation infrared (IR) spectroscopy with the aid of density functional theory (DFT) calculation. An IR spectrum measured after deposition was assigned to an enol isomer, the conformation of which is *anti* in relation to OH versus N in the pyridine ring. When the matrix sample was exposed to UV and visible light ($\lambda > 350$ nm), an IR spectrum consistent with a keto product was observed. During the irradiation, an IR spectrum of a transient species, a photoreaction intermediate between *anti*-enol and keto, was observed, which was assigned to *syn*-enol. The bands of *syn*-enol disappeared completely when the irradiation was stopped, while those of the original isomer, *anti*-enol, reappeared. No reverse isomerization was observable in the corresponding deuterated species. This led to the conclusion that the isomerization from *syn* to *anti* occurs through hydrogen-atom tunneling. On the other hand, an *aci*-nitro form was produced by UV irradiation ($\lambda = 365 \pm 10$ nm) without visible light. The conformation around the *aci*-nitro group was determined to be cis−cis by comparison with the spectral patterns obtained by the DFT/B3LYP/6-31++G** calculation. The dynamics of the hydrogen-atom migrations between *anti*- and *syn*-enols, *syn*-enol and keto, and *anti*-enol and *aci*-nitro are discussed in terms of the potential surfaces obtained by the DFT calculation.

1. Introduction

2-Hydroxypyridine is one of the simplest model compounds for nucleic acids such as uracil and thymine. The intra- and intermolecular hydrogen bonds between the hydrogen atom in the OH group and a lone pair of the nitrogen atom play important roles in biological and chemical reactions. The intramolecular hydrogen-atom migration to the nitrogen atom produces a keto isomer, 2-pyridone (see Scheme 1). The keto−enol equilibrium has been investigated under various experimental conditions.[1−11] It is well-known that keto mainly exists in crystals[1−3] and in polar solutions,[4,5] while enol and keto coexist in diluted nonpolar solutions,[6] in the gas phase,[5,7−9] and in low-temperature rare-gas matrices.[10,11] The energy difference between the two isomers in the isolated states is reported to be a few kilojoules/mole, where enol is more stable than keto. Numerous quantum chemical calculations were also performed to predict the relative stability between keto and enol using various calculation methods and basis sets.[12−17] In contrast to the experimental results in the isolated states, some recent quantum chemical calculations lead to the conclusion that keto is more stable than enol. So far the inconsistency between the experimental and calculation results remains unsettled.

The enol isomer of 2-hydroxypyridine has two conformations around the C−O bond, i.e., *syn* and *anti* in relation to the OH group versus the N atom. Matsuda et al. obtained the relative energies for *syn* and *anti* at the HF/6-31G level and reported that *anti* is ca. 32 kJ mol^{-1} less stable than *syn* because *anti* is destabilized by the repulsion between the lone pairs of the oxygen and nitrogen atoms.[18] No experimental report on *anti* has yet been published.

SCHEME 1

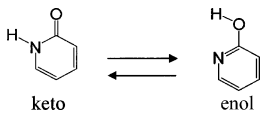

SCHEME 2

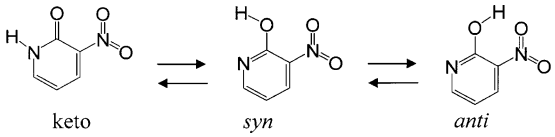

In the present study, 2-hydroxy-3-nitropyridine, hereafter called HNP, is a target molecule to be investigated. The keto−enol equilibrium of this molecule was previously studied by NMR spectroscopy,[5,19] which showed that keto mainly exists in the solution with a small amount of enol. The understanding of the keto−enol equilibrium in this molecule may be more complicated than that in 2-hydroxypyridine, because HNP has another intramolecular hydrogen bond of OH···ONO besides the O−H···N found in 2-hydroxypyridine. The stabilization caused by the OH···ONO intramolecular hydrogen bond should make *anti*-enol more stable than keto (see Scheme 2). One of the purposes of the present study is to examine the conformational change around the C−O bond in the matrix-isolation states with the keto−enol equilibrium.

The photoreaction mechanism of 2-nitrophenol has recently been investigated.[20,21] The vibrational assignments with the aid of the density functional theory (DFT) calculation lead to the

* Corresponding author. Fax: +81-42-388-7349. E-mail: necom@cc.tuat.ac.jp.

10.1021/jp0726687 CCC: $37.00
Published on Web 06/26/2007

SCHEME 3

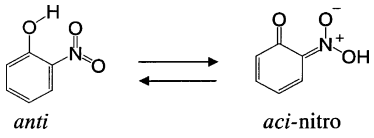

conclusion that an *aci*-nitro form was produced by the hydrogen-atom migration from the OH group to the nitro group upon UV irradiation (see Scheme 3). In the present study, we examine the three kinds of hydrogen-atom migrations in HNP by low-temperature matrix-isolation infrared (IR) spectroscopy and the DFT calculation method: between (1) enol and keto, (2) *anti*- and *syn*-enols, and (3) enol and *aci*-nitro. These reaction pathways in relation to the intramolecular hydrogen bonds are complicated, but the matrix-isolation technique combined with the DFT method should make it possible to elucidate the hydrogen-atom migrations in HNP, since the observed IR bands are sharp enough to distinguish each of the isomers in dense spectra.

2. Experimental and Calculation Methods

A sample of HNP was purchased from Tokyo Chemical Industry Co. Ltd. A deuterated sample was synthesized by mixing HNP in acetone with an excess amount of D_2O. Each sample placed in a deposition nozzle with a heating system was vaporized at 370 K. Pure argon (Nippon Sanso, 99.9999%) was flowed over the sample, and the flow rate of argon gas was adjusted to obtain sufficient isolation. The mixed gas was expanded through a stainless steel pipe of 1/16 in. in diameter and deposited in a vacuum chamber on a CsI plate, cooled at 20 K by a closed-cycle helium refrigerator unit (CTI Cryogenics, model M-22). UV radiation from a superhigh-pressure mercury lamp (Ushio, SX-UI-500HQ) was used to induce photoisomerization, where a water filter was used to remove thermal reactions and U330, UV36 (HOYA), L42 (Toshiba), and CVI (CVI Laser) optical filters adjusted the irradiation wavelength. IR spectra of the matrix sample were measured with an FTIR spectrophotometer (JEOL, model JIR-7000). The band resolution was 0.5 cm^{-1}, and the number of accumulation was four in the experiments on the tunneling reactions and 64 otherwise, where it takes ca. 4 s for one scan. Other experimental details were reported elsewhere.[22,23]

DFT calculations with the 6-31++G** basis set were carried out using the Gaussian03 program.[24] Beck's three-parameter hybrid density functional,[25] in combination with the Lee−Yang−Parr correlation functional (B3LYP),[26] was used to optimize the geometrical structures.

3. Results and Discussion

Quantum Chemical Calculations. Among many possible isomers of HNP, the geometries of one keto, two enols (*syn* and *anti*), and two *aci*-nitro forms [trans−cis (TC) and cis−cis (CC)] were optimized at the DFT/B3LYP/6-31++G** level of calculation (see Figure 1). The most stable isomer is *anti*-enol, the conformation of which is *anti* in relation to OH versus N in the pyridine ring. As described in the Introduction, the corresponding *anti*-enol of 2-hydroxypyridine has yet been undetectable, since it is destabilized by the repulsion between the lone pairs of the oxygen and nitrogen atoms. We optimized the geometries of 2-hydroxypyridine by a similar quantum chemical calculation and found that *anti* is less stable than *syn* by 22.4 kJ mol^{-1}. In contrast to 2-hydroxypyridine, *anti*-enol of HNP is more stable than *syn*-enol by 19.5 kJ mol^{-1}. This

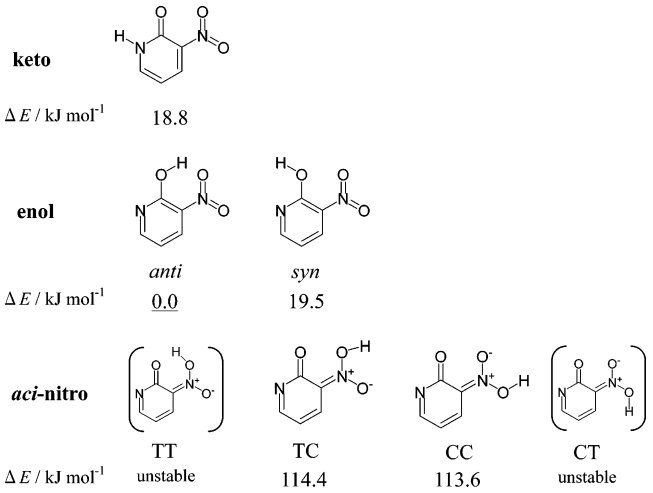

Figure 1. Possible isomers of HNP and their relative energies in kilojoules/mole calculated at the DFT/B3LYP/6-31++G** level.

stabilization is caused by the intramolecular hydrogen bond between the OH and ONO groups. The stabilization energy can be estimated to be 41.9 kJ mol^{-1} as the sum of 22.4 and 19.5 kJ mol^{-1}. This value is nearly equal to the energy difference between *syn* and *anti* of 2-nitrophenol, 44.8 kJ mol^{-1}.[20] Then we conclude that the intramolecular hydrogen bond of OH··· ONO in HNP is as strong as that in 2-nitrophenol. The influence of the hydrogen bond appears in the results of calculation on the O−H bond, where the distance of *anti*-enol, 0.986 Å, is 0.014 Å longer than that of *syn*-enol.

The second stable isomer is keto (see Figure 1). The relative energy against *anti*-enol, calculated to be 18.8 kJ mol^{-1}, is nearly equal to that of *syn*-enol, 19.5 kJ mol^{-1}. This is consistent with the results on 2-hydroxypyridine obtained by the DFT calculations, where the corresponding keto is a few kilojoules/mole more stable than *syn*-enol. The ONO planes for keto and *syn*-enol of HNP are out of the pyridine-ring plane, the torsional angles around the C−N bond being 27° and 12° respectively, implying that these isomers are destabilized by the repulsion between the lone pairs of the oxygen atoms in ONO and OH or C═O. It is noted that *anti*-enol of HNP is planar due to the intramolecular hydrogen bond and more stable than *syn*-enol and keto.

The *aci*-nitro form has two conformations around the C═N and N−OH bonds, resulting in four isomers. We call them TT, TC, CC, and CT, as defined in 2-nitrophenol.[20] The optimized geometries of two isomers, TC and CC, were obtained by the DFT calculations, where their relative energies against *anti*-enol were ca. 114 kJ mol^{-1}. On the other hand, CT and TT are transient structures; the former changed to CC without any potential barriers in optimization when it was assumed as an initial geometry in any input data, while the latter changed to *anti*-enol by an intramolecular hydrogen-atom migration.

IR Spectrum of *anti*-Enol. An IR spectrum of HNP in an argon matrix measured before irradiation is shown in Figure 2a. A broad band was observed at 3234 cm^{-1} in the O−H stretching region. This wavenumber is ca. 300 cm^{-1} lower than those of normal O−H stretching modes, implying that HNP has a strong hydrogen bond. Then we assigned the observed bands to *anti*-enol, which has an intramolecular hydrogen bond of OH·· ·ONO. The calculated spectral pattern of *anti*-enol obtained by the DFT calculation reproduces the observed spectrum satisfactorily, as shown in Figure 2b, although the observed one shows splitting due to Fermi resonance and a few additional bands due to combination modes. Since neither free O−H

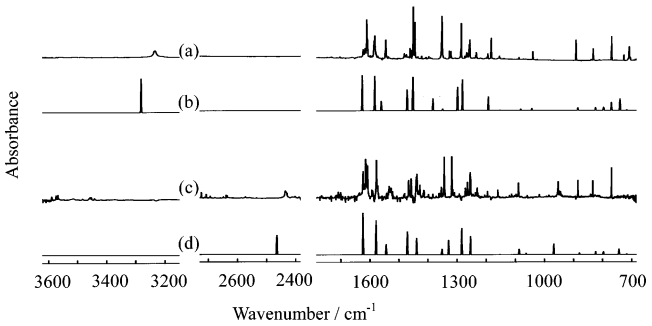

Figure 2. Observed and calculated IR spectra of *anti*-enol and its deuterated species: (a) observed IR spectrum of normal species measured after deposition, (b) calculated spectral pattern of normal *anti*-enol, (c) observed IR spectrum of deuterated species after deposition, and (d) calculated spectral pattern of deuterated *anti*-enol. Scaling factors of 0.95 and 0.98 are used in the regions higher and lower than 3000 cm^{-1}, respectively, in b and d.

stretching band nor free N−H stretching band was observed in the observed spectrum, the amounts of *syn*-enol and keto seem to be negligible in the matrix. This result is supported by the population ratio of *anti*-enol, 99.5%, estimated from the calculated relative energies based on the assumption of the Boltzmann distribution law at the deposition temperature of 370 K. The observed and calculated wavenumbers and relative intensities are summarized in Table 1.

To confirm our assignments further, we performed a similar experiment using a deuterated sample. The observed IR spectrum is compared with the calculated spectral pattern of deuterated *anti*-enol in Figure 2c,d. The O−D stretching band with a broadening due to the hydrogen bond was observed at 2436 cm^{-1}. The observed and calculated wavenumbers for the deuterated species are summarized in Table 1 with those for the normal species.

IR Spectra of Keto and a Transient Species, *syn*-Enol. When the matrix sample was exposed to UV and visible light through a UV36 short-wavelength cutoff filter (λ > 350 nm), a spectral change was observed. A difference spectrum between the spectra measured after irradiation minus that before 10-min irradiation is shown in Figure 3a, where the band intensities of the reactant, *anti*-enol, and a product decreased and increased, respectively. The strongest band of the product appearing at 1733 cm^{-1} is assignable to the C═O stretching mode and the 3419 cm^{-1} band to the N−H stretching mode. Then we tentatively identified the product as keto. The calculated spectral pattern of keto shown in Figure 3b reproduces the increasing bands satisfactorily within ca. 20 cm^{-1}, as summarized in Table 2. It is noted that this photoisomerization from enol to keto is in the opposite direction to that of the parent molecule, 2-hydroxypyrinde, in a low-temperature matrix reported by Nowak et al.[10]

The hydrogen atom in the OH group for *anti*-enol is located at a long distance from the nitrogen atom in the pyridine ring, while the corresponding hydrogen atom for *syn*-enol is close to the nitrogen atom. One may consider that the hydrogen-atom migration to produce keto occurs in *syn*-enol instead of *anti*-enol after the rotational isomerization around the C−O bond from *anti*-enol to *syn*-enol. This idea is reasonable because the potential barrier from *syn*-enol to keto, ca. 150 kJ mol^{-1}, is lower than the photon energy used in this experiment, ca. 350 kJ mol^{-1}, but the dissociation energy of hydrogen atom for the direct isomerization from *anti*-enol to keto, over 400 kJ mol^{-1}, is higher than the photon energy. To obtain an answer to the question whether *syn*-enol is a photoreaction intermediate between *anti*-enol and keto or not, we tried to measure an IR spectrum of a transient species existing only during UV and visible-light irradiation.

TABLE 1: Observed and Calculated Wavenumbers of *anti*-Enol

normal				deuterated			
obsd		calcd		obsd		calcd	
$\tilde{\nu}$	int[a]	$\tilde{\nu}^b$	int[c]	$\tilde{\nu}$	int[a]	$\tilde{\nu}^b$	int[c]
3234	m	3282	94				
		3079	1			3078	1
		3062	1			3062	1
		3021	6			3021	5
				2436	m	2465	46
1611	s	1627	100	1612	s	1624	100
1585, 1583	s	1584	98	1578, 1573	s	1579	82
1545	m	1561	27	1534, 1526	m	1544	25
1482	w						
1461	w	1472	60	1466, 1458	s	1471	56
1451, 1446	s	1452	95	1437	s	1439	40
1352	s	1383	34				
1327, 1320	w	1350	5	1354, 1345	s	1352	14
				1317	s	1329	35
1286	s	1299	66				
1273, 1267, 1257	s	1282	88	1271, 1264, 1254	s	1284	63
				1230	w	1254	44
1234	w						
1195, 1183	m	1193	39				
1155	w	1153	1	1155	w	1153	1
1088	w	1082	4	1098, 1089	m	1087	13
1040	m	1044	6	1062	w	1063	3
980	w	978	<1	980	w	978	<1
967	w	973	<1			972	<1
				953, 946	m	968	25
892	m	886	8	885	m	880	4
833	m	825	9	834	m	824	7
811	w	797	9	811	w	797	7
708	m	770	23				
769	m	741	33	769	s	744	13
727	w	717	2	727	w	717	1
675	w	673	2	673	w	672	2

[a] Letters represent relative intensities; s, m, and w denote strong, medium, and weak, respectively. [b] Calculated at DFT/B3LYP/6-31++G** level. Scaling factors of 0.95 and 0.98 are used in the regions above and below 3000 cm^{-1}, respectively. [c] Relative intensities.

Figure 4a shows a difference spectrum between the spectra measured *during* irradiation minus that *before* UV and visible-light irradiation through a UV36 short-wavelength cutoff filter (λ > 350 nm). The increasing bands marked with solid squares are due to keto, which is not a transient species but the final product. The other increasing bands are due to a transient species existing only during UV and visible-light irradiation. They completely disappeared when the irradiation on the matrix sample was stopped, as shown in the difference spectrum between the spectra measured *after* irradiation minus that *before* irradiation (see Figure 3a). On the other hand, the difference spectrum between the spectra measured *after* irradiation minus that *during* irradiation in Figure 4b displays that the bands for the transient species decrease and those for the original isomer, *anti*-enol, increase. These findings suggest one possibility that

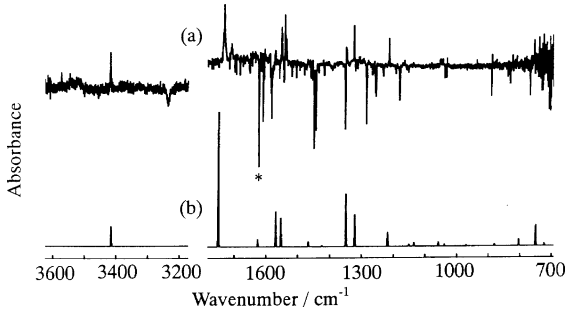

Figure 3. Observed and calculated IR spectra of keto: (a) observed difference spectrum between the spectra measured after irradiation minus that before irradiation of 10-min UV and visible light ($\lambda > 350$ nm) and (b) calculated spectral pattern of keto, where scaling factors of 0.95 and 0.98 are used in the regions higher and lower than 3000 cm^{-1}, respectively. The band marked with ∗ is due to H_2O in the matrix.

TABLE 2: Observed and Calculated Wavenumbers of Keto

obsd		calcd		obsd		calcd	
$\tilde{\nu}$	int[a]	$\tilde{\nu}^b$	int[c]	$\tilde{\nu}$	int[a]	$\tilde{\nu}^b$	int[c]
3419	s	3415	14			1151	2
		3087	<1	1141	w	1135	3
		3062	<1	1054	w	1058	3
		3059	<1	1047	w	1039	1
1733	s	1750	100			970	1
1712						939	<1
1600	w	1626	6	890	w	881	2
1554	m	1569	26	818	w	804	5
1543	s	1553	21	812	w		
1538						780	<1
1473	w	1467	4	756	m	750	15
		1425	1	719	w	723	2
1350	m	1349	39	686	w	687	4
1326	m	1321	24	649	w	647	2
1216	m	1218	10				

[a] Letters represent relative intensities; s, m, and w denote strong, medium, and weak, respectively. [b] Calculated at DFT/B3LYP/6-31++G** level. Scaling factors of 0.95 and 0.98 are used in the regions above and below 3000 cm^{-1}, respectively. [c] Relative intensities.

the transient species changes to keto by absorption of the second photon but returns immediately to *anti*-enol without photons. This transient species has a split band at 3553 and 3546 cm^{-1}, which is assignable to a free O−H stretching mode. Then we have identified this transient species as *syn*-enol. The calculated spectral pattern of *syn*-enol, shown in Figure 4c, is consistent with the decreasing bands for the transient species in Figure 4b.

A similar experiment for the deuterated sample was performed. A difference spectrum between the spectra measured *after* irradiation minus that *before* UV and visible-light irradiation ($\lambda > 350$ nm) is shown in Figure 5a, where the increasing and decreasing bands are due to the product and the reactant, respectively. We had first expected that deuterated keto was produced by the deuterium migration from the OD group to the N atom in the pyridine ring like normal species. However, the product has a split band appearing at 2623 and 2610 cm^{-1} in the O−D stretching region, which corresponds to the O−H stretching band of normal *syn*-enol. In addition, the product has no band in the C═O stretching region around 1700 cm^{-1}. Then we tentatively identified the product as *syn*-enol instead of keto. This identification has been confirmed by comparison of the increasing bands in Figure 5a with the spectral patterns of deuterated *syn*-enol in Figure 5b and keto in Figure 5c. Thus, we conclude that deuterated *syn*-enol was produced instead of keto as the final product instead of a transient species. This

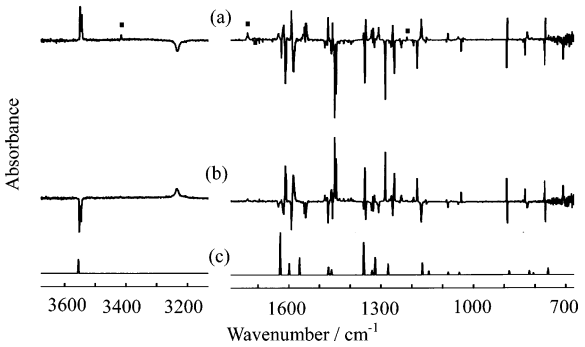

Figure 4. Observed and calculated IR spectra of *syn*-enol: (a) difference spectrum between the spectra measured *during* irradiation minus that *before* UV and visible-light irradiation ($\lambda > 350$ nm), (b) difference spectrum between the spectra measured *after* irradiation minus that *during* the irradiation, and (c) calculated spectral pattern of *syn*-enol, where scaling factors of 0.95 and 0.98 are used in the regions higher and lower than 3000 cm^{-1}, respectively. Bands marked with ■ represent keto.

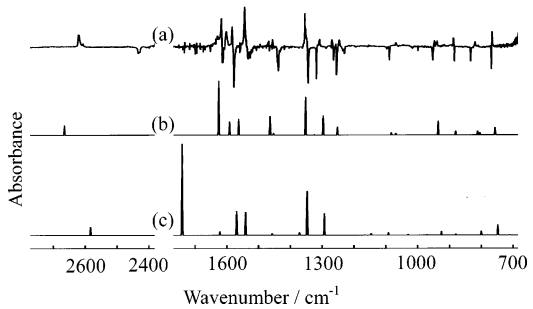

Figure 5. Observed and calculated IR spectra of deuterated *syn*-enol: (a) difference spectrum between the spectra measured after irradiation minus that before 5-min irradiation of UV and visible-light ($\lambda > 350$ nm) and (b and c) calculated spectral patterns of deuterated *syn*-enol and deuterated keto, respectively.

significant isotope effect is discussed below in terms of tunneling reactions. The observed and calculated wavenumbers and relative intensities for normal and deuterated species of *syn*-enol are summarized in Table 3.

IR Spectrum of *aci*-Nitro Form and Reverse Isomerization. When the matrix sample was exposed to UV light emitted from a superhigh-pressure mercury lamp through a U330 optical band-pass filter (220 nm < λ < 410 nm), the bands of a new photoproduct appeared with a decrease in the *anti*-enol bands. Figure 6a shows a difference spectrum between the spectra measured after irradiation minus that before UV irradiation without visible-light irradiation. The bands marked with solid squares are due to keto, as assigned in the previous section. The increasing bands marked with † are due to a new photoproduct. When the matrix sample was exposed to visible light through an L42 optical cutoff filter ($\lambda > 410$ nm) following the UV irradiation (220 nm < λ < 410 nm), a reverse isomerization to the original isomer, *anti*-enol, was observed, as shown in Figure 6b, where the keto bands marked with solid squares are unchanged. A similar reversible isomerization was found in 2-nitrophenol;[20] an *aci*-nitro form was produced from 2-nitirophenol by UV irradiation and returned to the original isomer by visible-light irradiation. Since this new product has the 3510 cm^{-1} band assignable to the free O−H stretching mode and the strong bands at 1700, 1514, 1296, and 938 cm^{-1} corresponding to the bands (1678, 1522, 1292, and 930 cm^{-1}) of the *aci*-nitro form of 2-nitrophenol, we identified the new product as the *aci*-nitro form of HNP. The calculated spectral patterns for the CC and TC isomers of *aci*-nitro are compared

TABLE 3: Observed and Calculated Wavenumbers of *syn*-Enol

normal				deuterated			
obsd		calcd		obsd		calcd	
$\tilde{\nu}$	int[a]	$\tilde{\nu}^b$	int[c]	$\tilde{\nu}$	int[a]	$\tilde{\nu}^b$	int[c]
3553 3546	s	3667	34				
						3178	1
		3178	1			3160	1
		3160	1			3124	3
		3124	3				
				2623 2610	m	2667	18
1638 1616	m	1628	100	1618 1604	s	1626	100
1592	s	1599	27	1583	m	1592	25
1547 1545	s	1565	41	1545	s	1563	30
1471	s	1471	19	1469	w	1464	35
1457	m	1461	13	1456	w	1453	3
1349	s	1356	77	1354	s	1352	70
1330	m	1329	11				
1307	m	1319	42	1308	w	1325	1
1262	m	1277	26	1269	w	1297	36
				1246	w	1252	15
1170 1168	s	1166	29				
1152	w	1145	9	1154	w	1150	<
1083	m	1082	7			1083	4
1049	w	1046	6	1070	w	1069	3
		981	1			981	1
		968	<1			968	<1
				948 943 940	w	936	26
890	s	884	10	888	w	881	7
831	m	819	10	821	w	812	8
825	w	806	5	811	w	805	4
767	s	758	16	767	m	757	14

[a] Letters represent relative intensities; s, m, and w denote strong, medium, and weak, respectively. [b] Calculated at DFT/B3LYP/6-31++G** level. Scaling factors of 0.95 and 0.98 are used in the regions above and below 3000 cm^{-1}, respectively. [c] Relative intensities.

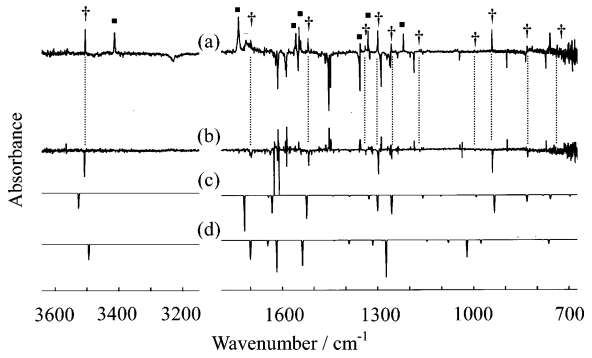

Figure 6. Observed and calculated IR spectra of *aci*-nitro form: (a) observed difference spectrum between the spectra measured after irradiation minus that before 5-min irradiation of UV (220 nm < λ < 410 nm), (b) difference spectrum between the spectra measured after irradiation minus that before 5-min irradiation of visible light (λ > 410 nm) following the measurement of a, c, and d calculated spectral patterns of CC and TC of *aci*-nitro form, respectively. Scaling factors of 0.95 and 0.98 are used in the regions higher and lower than 3000 cm^{-1}, respectively. Symbols of † and ■ represent CC of *aci*-nitro form and keto, respectively.

with the observed spectrum in Figure 6, resulting in that CC reproduces the observed bands marked with † more satisfactorily than TC. The reason why TC is undetectable is that it easily

TABLE 4: Observed and Calculated Wavenumbers of *aci*-Nitro Form

CC				TC		CC				TC	
obsd		calcd		calcd		obsd		calcd		calcd	
$\tilde{\nu}$	int[a]	$\tilde{\nu}^b$	int[c]	$\tilde{\nu}^b$	int[c]	$\tilde{\nu}$	int[a]	$\tilde{\nu}^b$	int[c]	$\tilde{\nu}^b$	int[c]
3510	s	3528	43	3495	49	1253	m	1255	53	1273	116
		3085	1	3073	1	1166	m	1157	9	1145	5
		3056	1	3055	1			1101	3	1078	9
		2981	8	3075	9	993	w	990	5	1020	54
1700 1695	m	1718	100	1700	60			976 967	<1 <1	978 976	<1 12
		1642	6	1645	19	938	s	933	50	973	<1
1636	s	1631	49	1617	100	829	m	831	19	880	1
1514	s	1522	65	1536	79			780	3	781	1
1436	w	1439	3	1436	3	751	w	757	12	763	13
1383	w	1387	4	1389	12			695	4	701	1
1335	m	1326	11	1315	17			637	<1	647	1
1296	s	1299	44	1284	2						

[a] Letters represent relative intensities; s, m, and w denote strong, medium, and weak, respectively. [b] Calculated at DFT/B3LYP/6-31++G** level. Scaling factors of 0.95 and 0.98 are used in the regions above and below 3000 cm^{-1}, respectively. [c] Relative intensities.

changes to TT by rotation around the N−OH bond in vibrational relaxation and then immediately to the original *anti*-enol by the migration of hydrogen atom with no essential potential barrier. A similar discussion has been made on the results of the photoreaction of 2-nitrophenol.[20] The observed wavenumbers are consistent with the calculated values of CC within 20 cm^{-1}, as summarized in Table 4 with the relative intensities. The IR spectrum of CC was also observed using a CVI band-pass filter (355 nm < λ < 375 nm), similarly to 2-nitrophenol.[20]

Photoreaction Mechanism. The above-mentioned photoreaction mechanisms of HNP are summarized in Scheme 4. Only the most stable isomer, anti, exits in the gas phase and in the matrix. The *anti*-enol isomerizes to *aci*-nitro by the migration of H in the OH group to the nitro group upon irradiation of ca. 365 nm. The *aci*-nitro form returns to the original *anti*-enol by visible-light irradiation (λ > 410 nm). The *anti*-enol isomerizes to keto by UV and visible-light irradiation (λ > 350 nm) via an intermediate, *syn*-enol, produced by the rotation around the C−O bond.

Here, the question arises how the transient isomer *syn*-enol returns to the original isomer, *anti*-enol. As described before, *syn*-enol exists only during UV and visible-light irradiation and returns to *anti*-enol instead of keto by stopping the irradiation. We consider the three possibilities for this reverse isomerization as follows: (1) thermal isomerization caused by infrared radiation from the source of an FTIR spectrophotometer, (2) thermal isomerization over low potential barriers in low-temperature matrices, and (3) isomerization by hydrogen-atom tunneling.

It is known that the rotational isomerization around the O−H bonds in alcohols, carboxylic acids, and nitrous acids occurs by infrared radiation with wavenumbers higher than 3000 cm^{-1}.[27−31] To confirm the possibility of the infrared-induced isomerization in HNP, we measured the spectral changes under two experimental conditions: (i) continued exposure of the matrix sample to the infrared beam of an FTIR spectrophotometer and (ii) elimination of the IR beam by shielding all the windows of the vacuum chamber with a sheet of aluminum foil except in the measurement of the IR spectra. The number of spectral accumulation was decreased to 4 to minimize the influence of the IR beam. As a result, no difference was observed between the results obtained under the two experi-

SCHEME 4

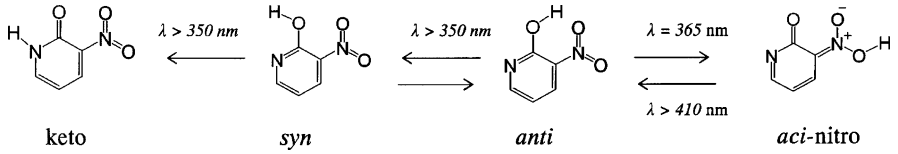

mental conditions. Thus we conclude that the reverse isomerization from *syn* to *anti* is not caused by IR radiation.

The thermal isomerization around the C−O bond in alcohols is possible even in low-temperature matrices, if the potential barrier is lower than 6 kJ mol^{-1}.[32] To distinguish thermal isomerization and tunneling isomerization, we tried to determine the rate constants for the isomerization of normal and deuterated species by an analysis of the kinetics. If the rate constant for the deuterated species is smaller than that of the normal species by a few orders of magnitude, tunneling isomerization is highly probable. Otherwise the isomerization from *syn* to *anti* occurs thermally over the potential barrier.

Figure 7 shows the absorbance changes of the normal *syn* (3553 cm^{-1}) and *anti* (1183 cm^{-1}) bands and the deuterated *syn* (2623 cm^{-1}) and *anti* (2436 cm^{-1}) bands after stopping the 5-min UV and visible-light irradiation ($\lambda > 350$ nm). The number of spectral accumulation was decreased to four since the isomerization rate was fast. The *syn* band at 3553 cm^{-1} and the *anti* band at 1183 cm^{-1} for the normal species rapidly decreased and increased, respectively, after stopping the irradiation. On the other hand, the deuterated *syn* band at 2623 cm^{-1} and the deuterated *anti* band at 2436 cm^{-1} were unchanged. We assumed the first-order reaction in a least-squares fitting and determined the rate constants to be 1.32 ± 0.06 and 0.0000 ± 0.0003 min^{-1} for the normal and deuterated species, respectively. The calculated absorbance is drawn in a solid line in Figure 7. Since the rate constant for the deuterated species is smaller than 0.0003 min^{-1}, i.e., $^1/_{1000}$ of that for the normal species, we conclude that the reverse isomerization from *syn* to *anti* is due to a hydrogen-atom tunneling reaction.

As mentioned in the foregoing, the isomerization from *syn*-enol to keto occurs upon UV and visible-light irradiation for the normal species. On the other hand, the spectral change due to this isomerization, as well as the reverse isomerization from *syn*-enol to *anti*-enol, was undetectable in the deuterated species, even when the matrix sample was exposed as long as 80 min. This remarkable isotope effect can be ascribed to a tunneling reaction, as found in the related compounds.[33−36] However, the tunneling reaction in the electronic ground state seems to be difficult because the potential barrier for the isomerization is too high, estimated to be 146 kJ mol^{-1} in our DFT calculations. Another possibility to explain the large isotope effect is a tunneling reaction in electronically exited states. Unfortunately, we have little information on the electronically excited states of HNP. This problem remains unresolved at the present stage.

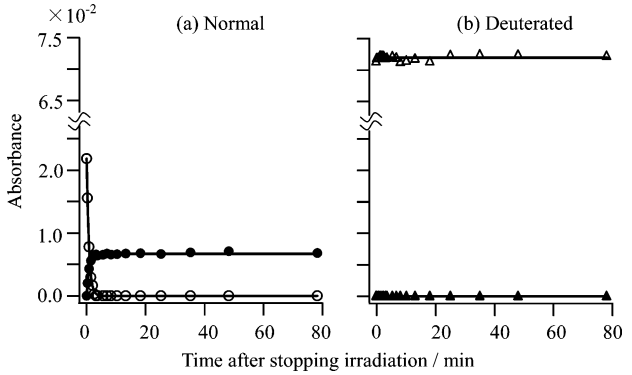

Figure 7. Absorbance changes of IR bands after stopping UV irradiation: (a) normal and (b) deuterated species. Symbols of ○, ●, △, and ▲ represent the absorbance for normal *syn*-enol (3553 cm^{-1}), normal *anti*-enol (1183 cm^{-1}), deuterated *syn*-enol (2623 cm^{-1}), and deuterated *anti*-enol (2436 cm^{-1}) bands, respectively. Solid lines represent the calculated values obtained by a least-squares fitting with an assumption of the first-order reaction.

4. Conclusion

A comparison of the IR spectrum measured after deposition with the calculated spectral patterns of 2-hydroxy-3-nitropyridine showed that *anti*-enol, with the conformation of *anti* in relation to OH versus N in the pyridine, exists in the gas phase and in the low-temperature matrices. No other isomers were detectable in the spectrum. When the matrix sample was exposed to UV light ($355 < \lambda < 375$ nm), the hydrogen atom in the OH group migrated to the nitro group to produce an *aci*-nitro form. The conformation of the *aci*-nitro group was assigned to CC, by comparison with the calculated spectral pattern. It was speculated from the results of the photoreaction of 2-nitrophenol that the other possible isomer, TC, was undetectable because it returned to the original isomer, *anti*-enol, through a transient isomer, TT, in vibrational relaxation. When the matrix sample was exposed to UV and visible light ($\lambda > 350$ nm), the hydrogen-atom migration around the C−O bond from the position of *anti* to that of *syn* occurred. By measuring the IR spectrum of a transient species existing only during irradiation of UV and visible light, it was concluded that keto was produced via *syn*-enol. The transient species, *syn*-enol, returned to the original isomer, *anti*-enol, immediately after termination of the irradiation, whereas the deuterated *syn* could not return. Therefore, we ascribed this reverse isomerization to the hydrogen-atom tunneling reaction.

Acknowledgment. The authors thank Prof. Kozo Kuchitsu (BASE, Tokyo University of A & T) for his helpful discussions.

References and Notes

(1) Penfold, B. *Acta Crystallogr.* **1953**, *6*, 591.
(2) Almof, J.; Kvick, A.; Fry, F. S., Jr. *Acta Crystallogr. B* **1971**, *27*, 1201.
(3) Wheeler, G. L.; Ammon, H. J. *Acta Crystallogr. B* **1974**, *30*, 680.
(4) De Kowalewski, D. G.; Contreras, R. H.; Díez, E.; Esteban, A. *Mol. Phys.* **2004**, *102*, 2607.
(5) Beak, P.; Fry, F. S., Jr.; Lee, J.; Steele, F. *J. Am. Chem. Soc.* **1976**, *98*, 171.
(6) Kuzuya, M.; Noguchi, A.; Okuda, T. *J. Chem. Soc. Chem. Commun.* **1984**, 435.
(7) Beak, P. *Acc. Chem. Res.* **1977**, *10*, 186.
(8) Brown, R. S.; Tse, A.; Vederas, J. C. *J. Am. Chem. Soc.* **1980**, *102*, 1174.
(9) Krebs, C.; Forster, W.; Weiss, C.; Hofmann, H. J. *J. Prakt. Chem.* **1982**, *324*, 369.
(10) Nowak, M. J.; Lapinski, L.; Les, A.; Adamowicz, L. *J. Phys. Chem.* **1992**, *96*, 1562.
(11) Dkhissi, A.; Houben, L.; Smets, J.; Adamowicz, L.; Maes, G. *J. Mol. Struct.* **1999**, *484*, 215.
(12) Sobolewski, A. L. *Chem. Phys. Lett.* **1993**, *211*, 293.
(13) Barone, V.; Adamo, C. *Chem. Phys. Lett.* **1994**, *226*, 399.

(14) Chou, P. T.; Wei, C. Y.; Hung, F. T. *J. Phys. Chem. B* **1997**, *101*, 9119.
(15) Li, Q. S.; Fang, W. H.; Yu, J. G. *J. Phys. Chem. A* **2005**, *109*, 3984.
(16) Fu, A.; Li, H.; Du, D.; Zhou, Z. *J. Phys. Chem. A* **2005**, *109*, 1468.
(17) Tsuchida, N.; Yamabe, S. *J. Phys. Chem. A* **2005**, *109*, 1974.
(18) Matsuda, Y.; Ebata, T.; Mikami, N. *J. Phys. Chem. A* **2001**, *105*, 3475.
(19) Kolehmainen, E.; Laihia, K.; Rasałła, D.; Gawinecki, R. *Magn. Reson. Chem.* **1991**, *29*, 878.
(20) Nagaya, M.; Kudoh, S.; Nakata, M. *Chem. Phys. Lett.* **2006**, *427*, 67.
(21) Chen, P. C.; Chieh, Y. C. *Chem. Phys. Lett.* **2003**, *372*, 147.
(22) Yaehata, H.; Nagaya, M.; Kudoh, S.; Nakata, M. *Chem. Phys. Lett.* **2006**, *424*, 279.
(23) Nagaya, M.; Kudoh, S.; Nakata, M. *Chem. Phys. Lett.* **2006**, *432*, 446.
(24) Frisch, M. J.; Trucks, G. W.; Schlegel, H. B.; Scuseria, G. E.; Robb, M. A.; Cheeseman, J. R.; Montgomery, J. A., Jr.; Vreven, T.; Kudin, K. N.; Burant, J. C.; Millam, J. M.; Iyengar, S. S.; Tomasi, J.; Barone, V.; Mennucci, B.; Cossi, M.; Scalmani, G.; Rega, N.; Petersson, G. A.; Nakatsuji, H.; Hada, M.; Ehara, M.; Toyota, K.; Fukuda, R.; Hasegawa, J.; Ishida, M.; Nakajima, T.; Honda, Y.; Kitao, O.; Nakai, H.; Klene, M.; Li, X.; Knox, J. E.; Hratchian, H. P.; Cross, J. B.; Adamo, C.; Jaramillo, J.; Gomperts, R.; Stratmann, R. E.; Yazyev, O.; Austin, A. J.; Cammi, R.; Pomelli, C.; Ochterski, J. W.; Ayala, P. Y.; Morokuma, K.; Voth, G. A.; Salvador, P.; Dannenberg, J. J.; Zakrzewski, V. G.; Dapprich, S.; Daniels, A. D.; Strain, M. C.; Farkas, O.; Malick, D. K.; Rabuck, A. D.; Raghavachari, K.; Foresman, J. B.; Ortiz, J. V.; Cui, Q.; Baboul, A. G.; Clifford, S.; Cioslowski, J.; Stefanov, B. B.; Liu, G.; Liashenko, A.; Piskorz, P.; Komaromi, I.; Martin, R. L.; Fox, D. J.; Keith, T.; Al-Laham, M. A.; Peng, C. Y.; Nanayakkara, A.; Challacombe, M.; Gill, P. M. W.; Johnson, B.; Chen, W.; Wong, M. W.; Gonzalez, C.; Pople, J. A. *Gaussian 03*, Revision B.04; Gaussian, Inc.,: Pittsburgh PA, 2003.
(25) Becke, A. D. *J. Phys. Chem.* **1993**, *98*, 5648.
(26) Lee, C.; Yang, W.; Parr, R. G. *Phys. Rev. B* **1988**, *37*, 785.
(27) Baldeschwieler, L. D.; Pimentel, G. C. *J. Chem. Phys.* **1960**, *33*, 1008.
(28) Shirk, A. E.; Shirk, J. S. *Chem. Phys. Lett.* **1983**, *97*, 549.
(29) Maçôs, E. M. S.; Khriachtchev, L.; Pettersson, M.; Fausto, R.; Räsänen, M. *J. Chem. Phys.* **2003**, *119*, 11765.
(30) Lotta, T.; Murto, J.; Räsänen, M.; Aspiala, A. *J. Mol. Struct.* **1984**, *114*, 333.
(31) Kudoh, S.; Takayanagi, M.; Nakata, M.; Ishibashi, T.; Tasumi, M. *J. Mol. Struct.* **1999**, *479*, 41.
(32) Barns, A. J. *J. Mol. Struct.* **1984**, *113*, 161.
(33) Maçôs, E. M. S.; Khriachtchev, L.; Pettersson, M.; Fausto, R.; Räsänen, M. *J. Chem. Phys.* **2004**, *121*, 15.
(34) Akai, N.; Kudoh, S.; Takayanagi, M.; Nakata, M. *Chem. Phys Lett.* **2002**, *356*, 133.
(35) Akai, N.; Kudoh, S.; Takayanagi, M.; Nakata, M. *J. Phys. Chem. A* **2002**, *106*, 11029.
(36) Akai, N.; Kudoh, S.; Nakata, M. *J. Phys. Chem.* **2003**, *107*, 3655.